Neural Comput & Applic (2013) 23:895–905
DOI 10.1007/s00521-012-1014-2

ORIGINAL ARTICLE

Nonnegative matrix factorization-based hyperspectral and panchromatic image fusion

Zhou Zhang · Zhenwei Shi

Received: 10 April 2012 / Accepted: 21 June 2012 / Published online: 7 July 2012

Abstract The fusion of hyperspectral image and panchromatic image is an effective process to obtain an image with both high spatial and spectral resolutions. However, the spectral property stored in the original hyperspectral image is often distorted when using the class of traditional fusion techniques. Therefore, in this paper, we show how explicitly incorporating the notion of "spectra preservation" to improve the spectral resolution of the fused image. First, a new fusion model, spectral preservation based on nonnegative matrix factorization (SPNMF), is developed. Additionally, a multiplicative algorithm aiming at get the numerical solution of the proposed model is presented. Finally, experiments using synthetic and real data demonstrate the SPNMF is a superior fusion technique for it could improve the spatial resolutions of hyperspectral images with their spectral properties reliably preserved.

Keywords Hyperspectral image fusion · Spectra preservation · Nonnegative matrix factorization (NMF) · Multiplicative algorithm

Z. Zhang · Z. Shi (✉)
Image Processing Center, School of Astronautics,
Beihang University, Beijing 100191, People's Republic of China
e-mail: shizhenwei@buaa.edu.cn

Z. Zhang
e-mail: zhangzhoubuaa@gmail.com

Z. Shi
Beijing Key Laboratory of Digital Media,
Beihang University, Beijing 100191, People's Republic of China

Z. Shi
State Key Laboratory of Virtual Reality Technology
and Systems, Beihang University, Beijing 100191,
People's Republic of China

1 Introduction

Hyperspectral remote sensing is a new type of remote sensing that has attracted many people's attention recently. The hyperspectral image is a kind of three-dimensional data: two spatial dimensions and one spectral dimension [1] and thus is called "data cube". For each pixel, the spectral dimension provides a continuous spectrum, which has been widely used in a variety of applications (such as target detection, identification of natural and man-made materials) [2]. However, due to the limitation of the imaging spectrometer, the hyperspectral data has low spatial resolution, which restricts the application of hyperspectral remote sensing in some fields. Instead, compared to the hyperspectral image, the panchromatic image has high spatial resolution while no spectral information. Therefore, the fusion of hyperspectral and panchromatic image data has a possibility to produce the fused data with high spatial and spectral resolutions.

There are several studies on fusion algorithms and the most common ones can be separated into three categories [3, 4]: (1) projection and substitution methods, such as intensity, hue and saturation transform (IHS) [5]; (2) different arithmetic combinations, such as Brovey's transform (BT) [6]; (3) the wavelet-based fusion methods and those methods that inject spatial information from panchromatic images into hyperspectral or multispectral images, such as discrete wavelet transform (DWT) [7] and high-pass filtering (HPF) [8].

IHS transformation can effectively separate spatial (intensity) and spectral (hue and saturation) information from a standard RGB image. To conduct an IHS image fusion, intensity component (I) should be replaced by the panchromatic image. If the intensity image of the IHS transform has a high correlation with the panchromatic image being used, it will produce a satisfactory fusion

result. However, in practice, the intensity image and the panchromatic image often differ from each other to a certain extend. Therefore, a common problem of the IHS technique is the color distortion [9, 10]. BT is an IHS-like method [11], and it is based on the chromaticity transform [12, 13]. It is a simple fusion method while it would also cause spectral distortion. Most literatures recognize that the main disadvantage of IHS and BT over other fusion techniques is that these two methods could only handle with three-band imagery [3, 4, 14]. Hence, they are not suitable to deal with the hyperspectral image, which involves much more than three bands.

Recently, many researchers have focused on image fusion using wavelet transformation [15, 16]. The wavelet-based fusion methods extract spatial detail information from a high-resolution panchromatic image and then inject it into the hyperspectral bands. In this manner, owing to the detailed information extracted from the panchromatic image differs from the existing information in the original hyperspectral image, the DWT method could also cause spectral distortion to some certain extend. The HPF is similar to the DWT, because they both inject the spatial features into the hyperspectral images during the fusion process. However, when we use the HPF method, the spatial features are extracted using high-pass filtering rather than the wavelet transform. These two methods have a prominent advantage, which is that they have the ability to handle images with arbitrary bands, such as the hyperspectral images.

In recent decades, nonnegative matrix factorization (NMF) which was first proposed by D.D. Lee and H.S. Seung in 1999 [17] has been successfully used in the field of hyperspectral image analysis and processing, such as in the spectral unmixing [18]. To unmix hyperspectral data, the original image cube can be decomposed into the spectral matrix and the abundance matrix by using the NMF technique. The hyperspectral images themselves often include large-scale data, generally stored in the form of matrices, and the identification and the analysis of them are also implemented in the form of matrices. In addition, it is obvious that the gray of pixels is always nonnegative. These characteristics make NMF indubitably become one popular technique for the hyperspectral image processing.

In this paper, we propose a new model called the spectral preservation based on nonnegative matrix factorization (SPNMF) for hyperspectral and panchromatic data fusion. In the fusion, we extract the feature of the hyperspectral data by NMF and enhance the feature with high spatial resolution image (panchromatic image). Besides, in this new model, a regularized term aiming at preserving the spectral information of the fused hyperspectral data is added based on the original NMF. By combining these two parts, fused hyperspectral data with both high spatial and spectral resolutions can be generated. In addition, both spatial and spectral reconstruction qualities are evaluated by three experiments using synthetic data and real data. The results of comparison with other two traditional methods—HPF and DWT—are also provided.

This paper is organized as follows. Section 2 describes the SPNMF model for the hyperspectral and panchromatic data fusion. Section 3 proposes the corresponding multiplicative algorithm, which is used to get the numerical solution of the proposed model. In Sect. 4, experimental results both on synthetic and real data with different hyperspectral image fusion methods are discussed and finally close with conclusions in Sect. 5.

2 Spectral preservation based on nonnegative matrix factorization (SPNMF) fusion model

The aim of hyperspectral and panchromatic data fusion is to obtain the image with both high spatial and spectral resolutions. Thus, we take into account of these two requirements in conducting the fusion model.

2.1 Nonnegative matrix factorization (NMF) for hyperspectral unmixing

Original nonnegative matrix factorization model is that given a nonnegative matrix $\mathbf{V}$ finds nonnegative matrix factors $\mathbf{W}$ and $\mathbf{H}$ such that:

$$\mathbf{V} \approx \mathbf{WH} \tag{1}$$

Here, to fuse the hyperspectral data, $\mathbf{V} \in \mathbb{R}^{L\times K}$ denotes the hyperspectral data that contains L bands and K pixels. Each row of $\mathbf{V}$ stands for one band of the original hyperspectral image. $\mathbf{W} \in \mathbb{R}^{L\times S}$ is the spectral signature matrix, with each column $\{\mathbf{w}_r\}_{r=1}^{P} \in \mathbb{R}^{L}$ representing the endmember spectrum (the spectrum of a pure object, such as tree, rive, roof …) and S representing the number of endmembers (the pure objects). $\mathbf{H} \in \mathbb{R}^{S\times K}$ is the abundance matrix, with each column $\{\mathbf{h}_j\}_{j=1}^{K} \in \mathbb{R}^{S}$ representing the fractions of all the endmembers at a certain pixel. Therefore, we can reconstruct the hyperspectral data $\mathbf{V}$ by using $\mathbf{V} \approx \mathbf{WH}$.

To ensure the result of reconstruction satisfying $\mathbf{V} \approx \mathbf{WH}$ for NMF, we simply use the square of the Euclidean distance [19] between $\mathbf{V}$ and $\mathbf{WH}$ as an objective function as follows:

$$\mathrm{Euc}(\mathbf{W},\mathbf{H}) = \frac{1}{2}||\mathbf{V}-\mathbf{WH}||^2 = \frac{1}{2}\sum_i\sum_j \left(\mathbf{V}_{ij} - \left(\mathbf{WH}_{ij}\right)\right)^2 \tag{2}$$

To get the solution of the NMF problem, Lee and Seung [17, 20] proposed a multiplicative update algorithm with nonincreasing behavior.

2.2 Spectral preservation based on NMF (SPNMF)

As we have discussed before, the proposed fusion model is designed to satisfy the two fusion requirements: high spatial and spectral resolutions. Now we illustrate the idea of the proposed model in detail.

First, we consider how to improve the spatial resolution of the hyperspectral image. As mentioned before, the abundance matrix $\mathbf{H}$ contains the details of the image. Therefore, injecting the spatial detailed information to $\mathbf{H}$ and using it to reconstruct the matrix $\mathbf{V}$ can help achieve the high spatial resolution purpose. Notice that the panchromatic image has the high spatial resolution and we can use it to make a fusion with $\mathbf{H}$. We use the weighted fusion method, which is a common method in the pixel-based level fusion. The proposed fusion process is illustrated in Fig. 1.

According to the process in Fig. 1, one part of the fusion model aiming at advancing the spatial resolution can be expressed as follows:

$$\begin{aligned} &\min \quad F(\mathbf{W},\mathbf{H}) = \frac{1}{2}||\mathbf{V}-\mathbf{WH}||^2 \\ &\text{s.t.} \quad \mathbf{W}\geq 0, \mathbf{H}\geq 0 \end{aligned} \tag{3}$$

Therefore, we have the fused data $\mathbf{V}_f$:

$$\mathbf{V}_f = \mathbf{W}(\alpha\mathbf{H} + (1-\alpha)\mathbf{P}) \tag{4}$$

where $\mathbf{P} \in \mathbb{R}^{S\times K}$ represents replication of the panchromatic data. Each row of $\mathbf{P}$ denotes the panchromatic image and there are totally S times of replications. α is the weighed coefficient.

Second, we should also consider the other important principle of the hyperspectral image fusion: spectra preservation. In the proposed fusion model, the spatial detail information from a high-resolution panchromatic image is added to the matrix $\mathbf{H}$. Because the injected information of the panchromatic image does not hold the same spectral quality with the original hyperspectral image, in this manner, the spectral information of the fused image is not equivalent to that existing in the original hyperspectral image and thus spectral distortion happens. To overcome this problem, we can make use of the inherent features of the data.

Based on the original NMF, many researchers have added some constrained terms in order to get more accurate factorizations. As a result, several new regularization NMF (RNMF) models were formed, such as nonnegative sparse coding (NNSC) [21], constrained nonnegative matrix factorization (CNMF) for hyperspectral unmixing [18]. Thus, adding a constraint term can help us make use of the inherent features of the data. We know that the original hyperspectral image has the good spectral character, and if we can find a regularized term to constrain the spectral difference between the original and fused hyperspectral images, the purpose of preventing the spectra from being drastically destroyed could be achieved.

Spectral angle mapper (SAM) [22] is an important assessment for the spectral dimension of the hyperspectral data, which is defined as $\text{SAM} = \arccos\left(\frac{\langle \mathbf{a},\mathbf{b}\rangle}{||\mathbf{a}||||\mathbf{b}||}\right)$, where $\mathbf{a},\mathbf{b}$ respectively represent the certain pixel's spectral vector before and after the fusion. The smaller the value of the SAM is, the better the performance of the spectral preservation has. Hence, SAM can be a useful constraint function to refrain from spectral distortion. In this paper, each pixel's SAM is defined as:

$$\text{SAM} = \arccos\left(\frac{\langle \mathbf{v}_{fi}, \mathbf{v}_i\rangle}{||\mathbf{v}_{fi}||||\mathbf{v}_i||}\right) \tag{5}$$

where $\mathbf{v}_{fi} \in \mathbb{R}^L$ is the i-th column of the fused data $\mathbf{V}_f$ and i represents the i-th pixel in the image. Similarly, $\mathbf{v}_i$ represents the i-th column of the original hyperspectral data and it has the same size with $\mathbf{v}_{fi}$. Then, we can calculate the sum of all the pixels' SAM:

$$\text{SAM\_sum} = \sum_{i=1}^{K} \arccos\left(\frac{\langle \mathbf{v}_{fi}, \mathbf{v}_i\rangle}{||\mathbf{v}_{fi}||||\mathbf{v}_i||}\right) \tag{6}$$

where K represents the number of the pixels. Consider that the anti trigonometric function in (6) is difficult to be implemented and we can simplify it by just using its cosine value instead. Therefore, we have:

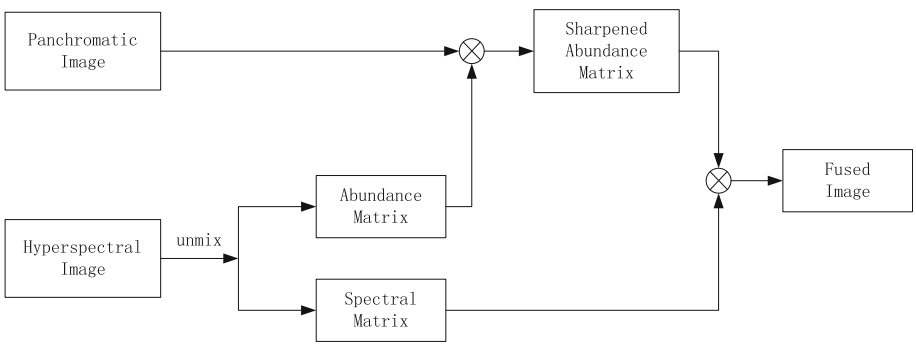

Fig. 1 Proposed fusion process

$$\text{SAM\_sum\_cos} = \sum_{i=1}^{K}\left(\frac{\langle \mathbf{v}_{fi}, \mathbf{v}_i\rangle}{||\mathbf{v}_{fi}||||\mathbf{v}_i||}\right) \tag{7}$$

To do the further simplification, we use the subtraction instead of the division and the quadratic style of (7) is chosen, then we have:

$$S(\mathbf{V}_f) = \sum_{i=1}^{K}\left(||\mathbf{v}_{fi}||^2||\mathbf{v}_i||^2 - \langle \mathbf{v}_{fi}, \mathbf{v}_i\rangle^2\right) \tag{8}$$

However, it is still not convenient for us to directly use (8) as the constraint function in the calculation and we transform it into the following formation, which is equivalent to (8).

$$S(\mathbf{V}_f) = \text{tr}\left((\mathbf{V}_f^{\mathrm{T}}\mathbf{V}_f)\odot(\mathbf{V}^{\mathrm{T}}\mathbf{V})\right) - \text{tr}\left(\left(\mathbf{V}_f^{\mathrm{T}}\mathbf{V}\right)\odot\left(\mathbf{V}_f^{\mathrm{T}}\mathbf{V}\right)\right) \tag{9}$$

where $\odot$ is the Hadamard (element-wise) product, $(\cdot)^{\mathrm{T}}$ denotes the transposition of the matrix and $\text{tr}(\cdot)$ represents the trace of the matrix. The function (9) is recognized as the final spectral constraint function. Adding (9) into the model (3), then we obtain the final fusion model:

$$\begin{aligned} &\min \quad J(\mathbf{W},\mathbf{H}) = F(\mathbf{W},\mathbf{H}) + \beta S(\mathbf{V}_f) \\ &\text{s.t.} \quad \mathbf{W}\geq 0, \mathbf{H}\geq 0 \end{aligned} \tag{10}$$

where β is a constant weight which is used to keep a balance between the spectral quality and the spatial quality of the fused image. $F(\mathbf{W},\mathbf{H})$ is defined in (3) and $S(\mathbf{V}_f)$ is defined in (9). Finally, we obtain the fused data

$$\mathbf{V}_f = \mathbf{W}(\alpha\mathbf{H} + (1-\alpha)\mathbf{P}) \tag{11}$$

This new proposed model improves the image's spatial resolution by using the panchromatic image $\mathbf{P}$. Simultaneously, the spectral character can be well preserved by the spectral constraint function $S(\mathbf{V}_f)$. In Sect. 3, we will discuss how to solve the optimization problem in (10) and (11).

3 Algorithm for SPNMF

To minimize the objective function (3), Lee and Seung [17, 20] proposed a multiplicative update algorithm, which was driven by carefully chosen the step-size of the gradient descent method. Since the factor matrices are updated only by multiplicative operations, they can remain in nonnegative during the iterations if they have been initiated with nonnegative numbers. The multiplicative update rules are given by

$$\mathbf{W} \longleftarrow \mathbf{W}\odot\frac{\mathbf{V}\mathbf{H}^{\mathrm{T}}}{\mathbf{W}\mathbf{H}\mathbf{H}^{\mathrm{T}}} \tag{12}$$

$$\mathbf{H} \longleftarrow \mathbf{H}\odot\frac{\mathbf{W}^{\mathrm{T}}\mathbf{V}}{\mathbf{W}^{\mathrm{T}}\mathbf{W}\mathbf{H}} \tag{13}$$

where $\odot$ denotes the Hadamard (element-wise) product and divisions are carried out in the element-wise way as well.

The multiplicative update rules can be derived from another way. The multiplication factor can be built by taking positive terms of the partial derivative as its denominator while taking negative ones as its numerator. According to (3), we have:

$$\begin{aligned} \frac{\partial F}{\partial \mathbf{W}} &= \left[\frac{\partial F}{\partial \mathbf{W}}\right]^{+} - \left[\frac{\partial F}{\partial \mathbf{W}}\right]^{-} \\ &= \mathbf{W}\mathbf{H}\mathbf{H}^{\mathrm{T}} - \mathbf{V}\mathbf{H}^{\mathrm{T}} \end{aligned} \tag{14}$$

Then the multiplicative update rule for $\mathbf{W}$ can be built like this:

$$\mathbf{W} \longleftarrow \mathbf{W}\odot\frac{[\partial F/\partial \mathbf{W}]^{-}}{[\partial F/\partial \mathbf{W}]^{+}} \tag{15}$$

It is similar to $\mathbf{H}$. Moreover, we can generalize it to construct the multiplicative update rule for an arbitrary factor matrix $\mathbf{U}$ like this:

$$\mathbf{U} \longleftarrow \mathbf{U}\odot\frac{[\partial F/\partial \mathbf{U}]^{-}}{[\partial F/\partial \mathbf{U}]^{+}} \tag{16}$$

The following update rules that we propose are derived in this way. From the objective function (10), we can calculate the partial derivative for matrix $\mathbf{W}$ and $\mathbf{H}$. We have:

$$\begin{aligned} \frac{\partial J}{\partial \mathbf{W}} &= (\mathbf{W}\mathbf{H}-\mathbf{V})\mathbf{H}^{\mathrm{T}} + 2\beta\mathbf{W}\mathbf{H}_0\text{diag}(\mathbf{V}^{\mathrm{T}}\mathbf{V})\mathbf{H}_0^{\mathrm{T}} \\ &\quad - 2\beta\mathbf{V}\text{diag}(\mathbf{H}_0^{\mathrm{T}}\mathbf{W}^{\mathrm{T}}\mathbf{V})\mathbf{H}_0^{\mathrm{T}} \end{aligned} \tag{17}$$

$$\begin{aligned} \frac{\partial J}{\partial \mathbf{H}} &= \mathbf{W}^{\mathrm{T}}(\mathbf{W}\mathbf{H}-\mathbf{V}) + 2\beta\alpha^2\mathbf{W}^{\mathrm{T}}\mathbf{W}\mathbf{H}\text{diag}(\mathbf{V}^{\mathrm{T}}\mathbf{V}) \\ &\quad + 2\beta\alpha(1-\alpha)\mathbf{W}^{\mathrm{T}}\mathbf{W}\mathbf{P}\text{diag}(\mathbf{V}^{\mathrm{T}}\mathbf{V}) \\ &\quad - 2\beta\alpha^2\mathbf{W}^{\mathrm{T}}\mathbf{V}\text{diag}(\mathbf{H}^{\mathrm{T}}\mathbf{W}^{\mathrm{T}}\mathbf{V}) \\ &\quad - 2\beta(1-\alpha)^2\mathbf{W}^{\mathrm{T}}\mathbf{V}\text{diag}(\mathbf{P}^{\mathrm{T}}\mathbf{W}^{\mathrm{T}}\mathbf{V}) \end{aligned} \tag{18}$$

where $(\cdot)^{\mathrm{T}}$ represents the transposition of the matrix. $\mathbf{H}_0 = \alpha\mathbf{H} + (1-\alpha)\mathbf{P}$. diag(*) is a diagonal matrix made up from the diagonal elements in matrix *.

Then the multiplicative update rules for $\mathbf{W}$ and $\mathbf{H}$ become

$$\begin{aligned} \mathbf{W} \longleftarrow \mathbf{W}\odot &(\mathbf{V}\mathbf{H}^{\mathrm{T}} + 2\beta\mathbf{V}\text{diag}(\mathbf{H}_0^{\mathrm{T}}\mathbf{W}^{\mathrm{T}}\mathbf{V})\mathbf{H}_0^{\mathrm{T}})\oslash \\ &(\mathbf{W}\mathbf{H}\mathbf{H}^{\mathrm{T}} + 2\beta\mathbf{W}\mathbf{H}_0\text{diag}(\mathbf{V}^{\mathrm{T}}\mathbf{V})\mathbf{H}_0^{\mathrm{T}}) \end{aligned} \tag{19}$$

$$\begin{aligned} \mathbf{H} \longleftarrow \mathbf{H}\odot &(\mathbf{W}^{\mathrm{T}}\mathbf{V} + 2\beta\alpha^2\mathbf{W}^{\mathrm{T}}\mathbf{W}\mathbf{P}\text{diag}(\mathbf{V}^{\mathrm{T}}\mathbf{V}) \\ &+ 2\beta\alpha^2\mathbf{W}^{\mathrm{T}}\mathbf{V}\text{diag}(\mathbf{H}^{\mathrm{T}}\mathbf{W}^{\mathrm{T}}\mathbf{V}) \\ &+ 2\beta(1-\alpha^2)\mathbf{W}^{\mathrm{T}}\mathbf{V}\text{diag}(\mathbf{P}^{\mathrm{T}}\mathbf{W}^{\mathrm{T}}\mathbf{V}))\oslash \\ &(\mathbf{W}^{\mathrm{T}}\mathbf{W}\mathbf{H} + 2\beta\alpha^2\mathbf{W}^{\mathrm{T}}\mathbf{W}\mathbf{H}\text{diag}(\mathbf{V}^{\mathrm{T}}\mathbf{V}) \\ &+ 2\beta\alpha\mathbf{W}^{\mathrm{T}}\mathbf{W}\mathbf{P}\text{diag}(\mathbf{V}^{\mathrm{T}}\mathbf{V})) \end{aligned} \tag{20}$$

where $\odot$ denotes the element-wise product and $\odot$ denotes the element-wise.

The initialization for the NMF-based methods may affect the results a lot since the NMF-based methods often result in the local minimum. In this paper, we use vertex component analysis (VCA) [23], which is a kind of unmixing method, to make the initialization for SPNMF.

Two stopping criteria for the algorithm are adopted. The first one is the maximum iteration number, which is set to 500 in our experiments. The second one is the cost function J should satisfy the following requirement

$$\left|\frac{J_{\text{old}} - J_{\text{new}}}{J_{\text{old}}}\right| \leq \text{tol} \tag{21}$$

where J_{old} represents the cost function's value of the last iteration, and J_{new} denotes the cost function's value of the current iteration. ϵ is set to 10^{-3} in our experiments.

Based on the update rules of $\mathbf{W}$ and $\mathbf{H}$, the algorithm for SPNMF is summarized below.

Algorithm 1 Spectral preservation based on nonnegative matrix factorization (SPNMF)

1: Initialize $\mathbf{W}$ and $\mathbf{H}$ by VCA.

2: Repeat

a) $J_{old} = J(\mathbf{W}, \mathbf{H})$

b) Update $\mathbf{W}$ by (19)

c) Update $\mathbf{H}$ by (20)

d) $J_{new} = J(\mathbf{W}, \mathbf{H})$

until the stopping criteria is satisfied.

4 Experimental results

In this section, we conduct three experiments by using one synthetic hyperspectral image and two real hyperspectral images. The proposed SPNMF algorithm is compared to other two popular methods: HPF and DWT. The parameters we choose for the SPNMF is $\beta = 10^{-3}$, tol $= 10^{-3}$, $\alpha = 0.4$. In order to make an objective evaluation, we use five image quality metrics here. Note that the experimental results depend on the initializations, and thus each experiment has been done ten times with the median values of the objective metrics as the final results.

4.1 Performance evaluation

To evaluate the performance of our proposed SPNMF algorithm, one possible approach is to examine the images visually in a qualitative manner. However, in order to compare the performances of different approaches, it is desirable to employ quantitative measures. The performance of hyperspectral and panchromatic data fusion is evaluated from two points: the spatial resolution of each spectral band image and the spectral quality of each spectrum at a single pixel [24]. Here, we introduce five typical metrics.

4.1.1 Spatial correction coefficient (SCC)

To judge the spatial quality of the fused images, we can compare the high frequency data from the panchromatic image to the high frequency data from each band of the fused image. To extract the high frequency data, the authors in both [25] and [13] used the high-pass filter given by

$$\text{mask} = \begin{bmatrix} -1 & -1 & -1 \\ -1 & 8 & -1 \\ -1 & -1 & -1 \end{bmatrix}$$

The high SCC between the fused image and the panchromatic image indicates that most of the spatial information of the panchromatic image is incorporated during the merging process. The ideal value is one.

4.1.2 Spectral angle mapper (SAM)

SAM is defined in expression (6). It has been widely used in hyperspectral image analysis to measure the spectral similarity between the fused image and the original hyperspectral image. SAM is recognized to be a global measurement of spectral distortion. Small angle indicates high similarity [26].

4.1.3 Spectral information divergence (SID)

SID can be used to describe the statistic of a spectrum, which is derived from the concept of divergence arising in information theory. It shows the spectral closeness between the fused and the original hyperspectral images at a pixel level [27]. Ideally, it should be close to zero. To compute SID, we have the vector $\mathbf{x} = (x_1, \ldots, x_N)^{\mathrm{T}}$, which is taken from the original hyperspectral image and $\mathbf{y} = (y_1, \ldots, y_N)^{\mathrm{T}}$ which is a vector from the final fused image. Then we have

$$p_j = \frac{x_j}{\sum_{i=1}^{N} x_i} \tag{22}$$

$$q_j = \frac{y_j}{\sum_{i=1}^{N} y_i} \tag{23}$$

where N is the number of bands. We define SID as:

$$SID(x, y) = D(x||y) + D(y||x) \tag{24}$$

where $D(x||y) = \sum_{i=1}^{L} p_i \log(p_i/q_i)$ and similarity for $D(y||x)$.

4.1.4 Q-average(Q)

The metric of the Q is defined as follows:

$$Q = \frac{4\sigma_{xy}\overline{x}\overline{y}}{(\sigma_x^2 + \sigma_y^2)[(\overline{x}^2) + (\overline{y}^2)]} \tag{25}$$

where $\overline{x}$ and $\overline{y}$ represent the average gray values of images x and y, respectively. σ_x and σ_y are the variances of images x and y, respectively. σ_{xy} is defined as $\frac{1}{N-1}\sum_{i=1}^{N}(x_i - \overline{x})(y_i - \overline{y})$. Q-average reflects the integration of three aspects: "loss of correlation, luminance distortion, and contrast distortion" [28] and its perfect value is one.

4.1.5 Relative dimensionless global error in synthesis (ERGAS)

The metric of the ERGAS is defined as follows:

$$\text{ERGAS} = 100\frac{h}{l}\sqrt{\frac{1}{L}\sum_{i=1}^{L}\frac{\text{RMSE}_i^2}{\mu_i^2}} \tag{26}$$

where h is the resolution of the high spatial resolution image, 1 is the resolution of the low spatial resolution image, μ_i is the mean radiance of each spectral band, L is the number of bands. RMSE is the root mean square error defined as follows [28]:

$$\text{RMSE} = \sqrt{\frac{1}{MN}\sum_{x=1}^{M}\sum_{y=1}^{N}(S(x,y) - F(x,y))^2} \tag{27}$$

where $S(x, y)$ and $F(x, y)$ are the standard and fused images, respectively. The value of ERGAS denotes the difference between the two images and it is expected to be zero.

4.2 Synthetic image experiment

In this experiment, we generated the synthetic data from the real airborne hyperspectral data. The real hyperspectral image was taken over an urban scene in Texas by the hyperspectral digital imagery collection experiment (HYDICE) sensor, which was composed of 210 bands with spectral resolution 10 nm acquired in the 400–2,400 nm region. We obtained data from the internet [29] with 1–100 bands and selected the sub-scene with the size of 307 × 306. First, we chose the image of band 4 as the image of panchromatic image for it had a comparative higher spatial resolution. Then, in order to get the experimental hyperspectral data, we down sampled the original hyperspectral data by a factor of 4 and resized it using the bilinear interpolation to make it has the same size as before. Therefore, in this experiment, the panchromatic image and the hyperspectral image have a fourfold difference in spatial resolution and both images were geometrically registered before the fusion.

4.2.1 Visual analysis

The original hyperspectral image, the panchromatic image and the fused images by different methods in false color with band 30, 60, 90 are shown in Fig. 2. Here, we choose the bands randomly to form the false color images. Figure 2a is the original hyperspectral image. Figure 2b is the panchromatic image. Figure 2c, d, e are the fused images yielded by HPF, DWT and SPNMF method, respectively.

It can be seen in Fig. 2 that all the fused images have better spatial features. Buildings, houses, streets and so on are easily identified in the fused images when using all these three methods and they share similar details. Besides, compared to the original hyperspectral image, the fused images obtained by these three methods seem all have good spectral fidelity. They all have good spectral and spatial performances on the visual evaluation and we cannot make clear comparison among these three fusion methods just by our naked eyes.

4.2.2 Statistical analysis

In order to analyze the performances of previous methods quantitatively, we evaluate them by using the five typical metrics mentioned before. The standard image for this experiment is the hyperspectral image we get from internet without being down sampled. Table 1 shows the objective metrics for the experiment 1. The bold font is the best one in the same row. From Table 1, it can be found that the fused image yielded by the SPNMF contains the most spatial detailed information because of the highest value of SCC. In term of the spectral fidelity, the proposed method SPNMF has the most desirable values in SAM, SID and Q, which are all used to evaluate the spectral performance. Besides, from the value of ERGAS, we can find that the SPNMF has the best performance among these three methods when considering the integration results of the two aspects: spatial and spectral resolutions.

4.3 Real image experiments

We conducted two groups of real image experiments. The hyperspectral data in the first experiment was acquired from the HJ1-A satellite, which composed of 110 bands [30] with a spatial solution of 100 m. After removing some bands with low signal–noise ratio, we used the remaining 100 bands to make the fusion. The panchromatic image was obtained from the google map [31] with the spatial resolution of 30 m. They were manually registered before

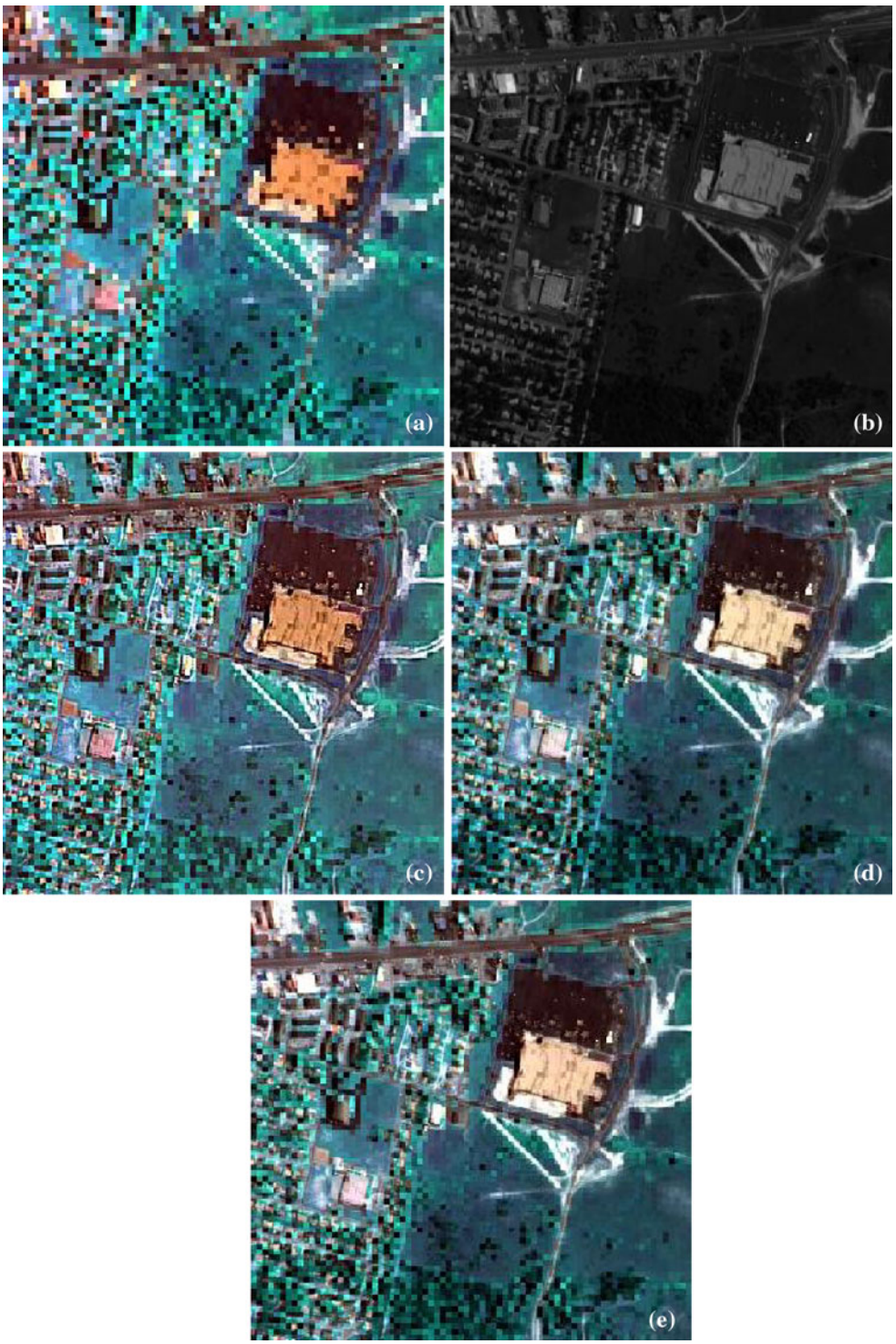

Fig. 2 Original images and fused images by using different methods. **a** Original hyperspectral image, **b** panchromatic image, **c** fused image by HPF, **d** fused image by DWT, **e** fused image by SPNMF

the experiment and they both had the size of 256 × 200. The second data to be used were obtained from the HYDICE sensor, which had been introduced in synthetic image experiment. We selected the sub-scene from the Washington, DC, with the size of 210 × 270. There were 64 bands remained after low-SNR bands removed. The corresponding panchromatic image was obtained from the google map [31] with the spatial resolution of 30 m.

Table 1 Objective metrics of synthetic image experiment

	HPF	DWT	SPNMF
SCC	0.7213	0.7360	**0.7564**
SAM	14.7368	8.5795	**5.9416**
SID	0.1669	0.0617	**0.0304**
Q	0.7331	0.7931	**0.8680**
ERGAS	15.7944	8.7573	**6.5192**

Bold values represent the best performance among the three methods under the same metric

4.3.1 Visual analysis

Here, we again use different methods to do the experiments. In the first real image experiment, the original hyperspectral image and fused images are shown in false color and we choose band 10, 40 and 70 to represent *R*, *G* and *B*, respectively. In the second experiment, the images are shown in false color with band 10, 30 and 50. We choose these bands randomly. Figures 3b and 4b represent the original hyperspectral image. The fused images obtained by the HPF, DWT, SPNMF are shown in Figs. 3c and 4c, Figs. 3d and 4d, and Figs. 3e and 4e, respectively. From Figs. 3 and 4, we can see that the fused images yielded by these three methods all have better spatial resolutions than those of the original hyperspectral images. We can see some useful detailed information clearly from them, such as the valleys in Fig. 3c, d, e, the streets and the buildings in Fig. 4c, d, e.

However, in terms of the spectral fidelity, these three methods perform differently. In the first real image

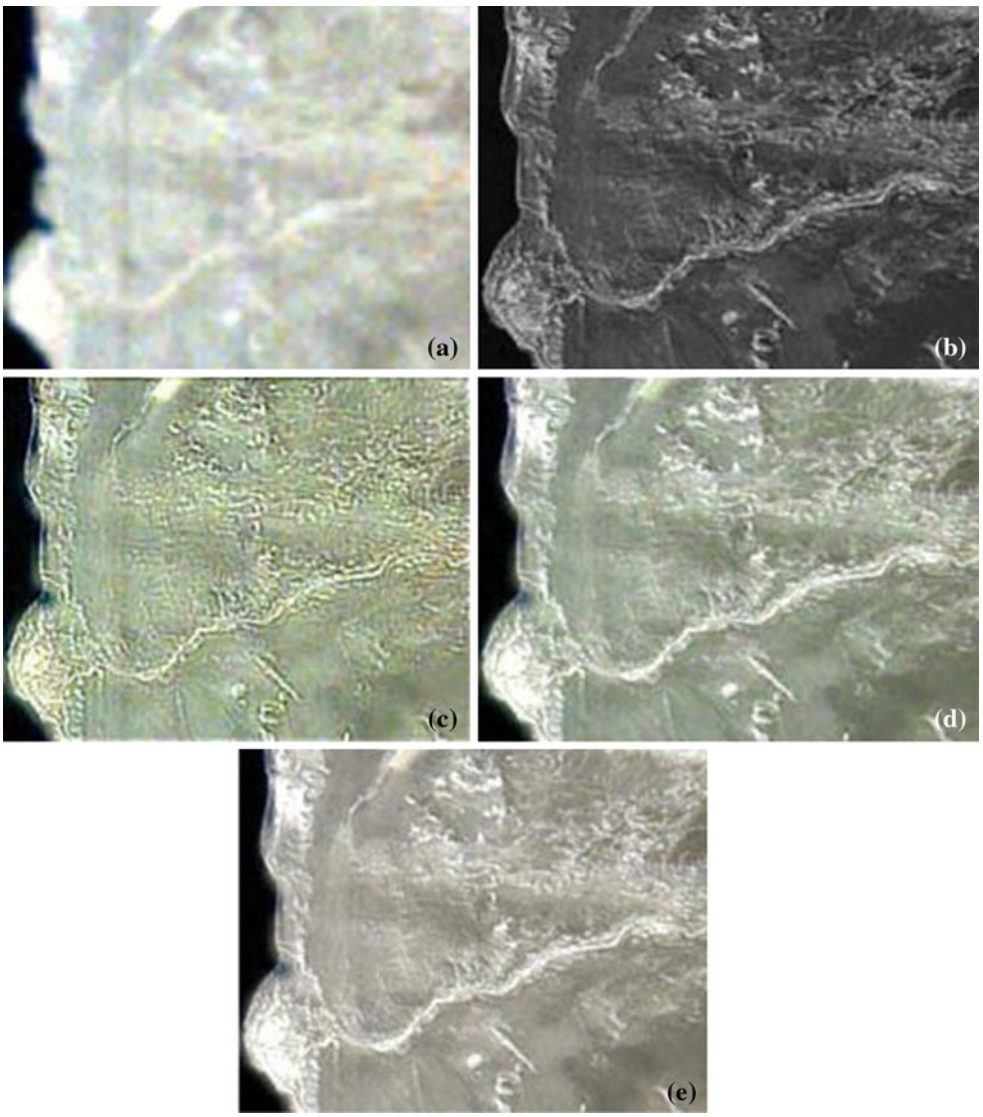

Fig. 3 Original images and fused false color images by using different methods. **a** original hyperspectral image, **b** panchromatic image, **c** fused image by HPF, **d** fused image by DWT, **e** fused image by SPNMF

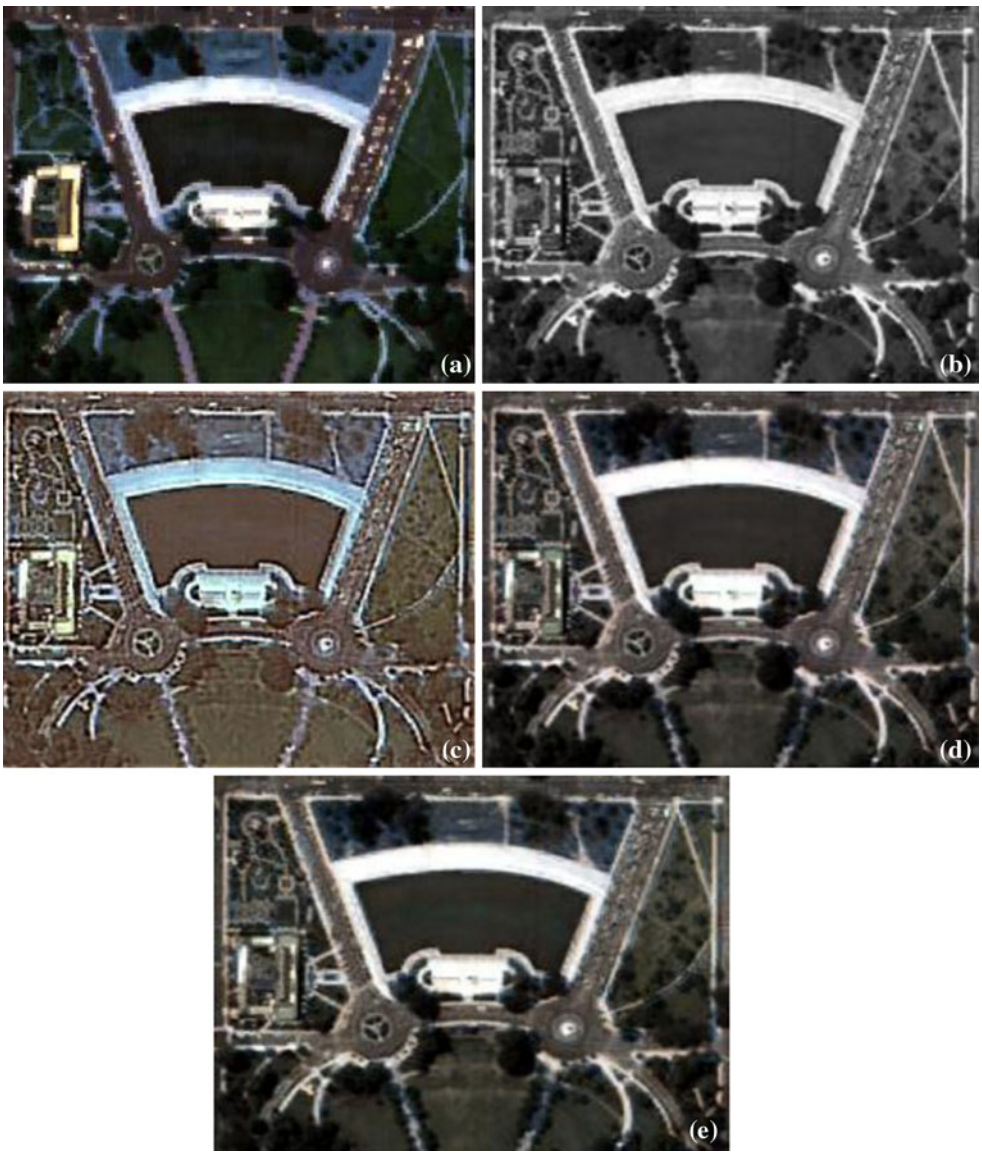

Fig. 4 Original images and fused images by using different methods. **a** original hyperspectral image, **b** panchromatic image, **c** fused image by HPF, **d** fused image by DWT, **e** fused image by SPNMF

experiment, the fused image obtained by the HPF (Fig. 3c) has obvious color distortion. The original gray image is turned into green. The image yielded by the DWT looks a little better than the one obtained by the HPF, but it still presents dark green in the whole image (see Fig. 3d). The SPNMF method overcomes the disadvantage of spectral distortion and it has similar color feature with the original hyperspectral image (see Fig. 3e). In the second real image experiment, the fused image obtained by the HPF (Fig. 4c) has obvious color distortion. It has excessive red in the vegetation and the color of the whole image seems unnatural. The fused images yielded by the DWT (Fig. 4d) and the SPNMF (Fig. 4e) both have good visual quality and we cannot differentiate the performances of these two methods just by our naked eyes.

4.3.2 Statistical analysis

Then, we use the objective metrics to make the evaluation as shown in Tables 2 and 3. In the Tables, the bold fond is the best one in the same row. The ERGAS metric is not listed here because it is impossible for us to find the standard image in the real image experiment. In the spatial aspect, from the values of SCC, we find that the proposed method SPNMF performs best in the first experiment. In general, the SPNMF method could inject much detail information from high-resolution image (panchromatic image) into the low-resolution image (hyperspectral image). In the second experiment, though the SPNMF does not perform as well as DWT in SID, based on the values of SAM, Q and SID in the first experiment, we can reliably

Table 2 Objective metrics of real image experiment 1

	HPF	DWT	SPNMF
SCC	0.9450	0.9790	**0.9825**
SAM	9.4524	8.7540	**3.5749**
SID	0.0435	0.0370	**0.0077**
Q	0.6102	0.7038	**0.7965**

Bold values represent the best performance among the three methods under the same metric

Table 3 Objective metrics of experiment 3

	HPF	DWT	SPNMF
SCC	0.8829	0.9204	**0.9618**
SAM	14.6115	12.3371	**10.5993**
SID	0.0996	**0.0695**	0.0882
Q	0.5086	0.4833	**0.5929**

Bold values represent the best performance among the three methods under the same metric

make the conclusion that the proposed method SPNMF has the best spectral quality among these three methods.

4.4 Experimental results analysis

In this paper, we use one group of synthetic data and two groups of real data to conduct the experiments. During the experiments, we compare the different performances of three methods: HPF, DWT and SPNMF. We find that these three methods all can improve the spatial resolution of the original hyperspectral image by making a fusion with the panchromatic image. In terms of the spectral preservation, we notice that the HPF performs well in the synthetic experiment image while behaves badly in the two groups of real image experiments, which indicates that the HPF method cannot always satisfy the requirement of spectral preservation in the hyperspectral image fusion. DWT has obvious spectral distortion in the first real image experiment and the proposed method SPNMF has comparatively better performances in these three experiments. Furthermore, after the evaluations by objective metrics, we can safely make the conclusion that the proposed method SPNMF could advance the spatial resolution of the original hyperspectral image, and in spectral preservation aspect, it is superior to other methods no matter in the synthetic image experiment or in the real image experiments.

5 Conclusions

In this paper, we propose a new model called spectral preservation based on nonnegative matrix factorization (SPNMF) based on the original NMF for the fusion between hyperspectral image and panchromatic image. To find the numerical solution of the fusion model, we change it into an optimization problem. Then we propose a multiplicative algorithm to solve the optimization problem. Three experiments including the synthetic hyperspectral image and the real hyperspectral images are conducted to evaluate the performances of different methods, and the comparisons among these methods are also analyzed. The results turn out that, contradicted to the traditional methods, the proposed SPNMF algorithm can advance the original hyperspectral image's spatial resolution and preserve the spectral information of the original hyperspectral image simultaneously. What is more, the SPNMF algorithm can be used both in the hyperspectral image fusion and the multispectral image fusion, because it has no limitation of the number of the bands. In sum, the SPNMF algorithm has a superior performance over some other traditional methods in dealing with the fusion between hyperspectral image and panchromatic image.

Acknowledgments The work was supported by the National Natural Science Foundation of China under the Grants 60975003 and 91120301, the 973 Program under the Grant 2010CB327904, the open funding project of State Key Laboratory of Virtual Reality Technology and Systems, Beihang University (Grant No. BUAA-VR-12KF-07), the Program for New Century Excellent Talents in University of Ministry of Education of China under the Grant NCET-11-0775, and the Beijing Natural Science Foundation (nonnegative component analysis for hyperspectral imagery unmixing) under the Grant 4112036.

References

1. Manolakis D, Marden D, Shaw GA (2003) Hyperspectral image processing for automatic target detection applications. Linc Lab 14(1):79–116
2. Shaw GA, Burke HK (2003) Spectral imaging for remote sensing. Linc Lab 14(1):3–28
3. Cetin M, Musaolu N (2009) Merging hyperspectral and panchromatic image data: qualitative and quantitative analysis. Int J Remote Sens 30(7):1779–1804
4. Zhang Y, Hong G (2005) An IHS and wavelet integrated approach to improve pan-sharpening visual quality of natural colour IKONOS and QuickBird images. Inf Fus 6:225–234
5. Carper WJ, Lillesand TM, Kiefer RW (1990) The use of intensity hue saturation transformations for merging SPOT panchromatic and multi-spectral image data. Photogramm Eng Remote Sens 56:459–467
6. Gillespie AR, Kahle AB, Walker RE (1987) Color enhancement of highly correlated imagesII. Channel ratio and chromaticity transformation techniques. Remote Sens Environ 22:343–365
7. King RL, Wang J (2001) A wavelet based algorithm for pan sharpening landsat 7 imagery. In: Proceedings of international geoscience and remote sensing symposium (IGARSS 2001), pp 849–851
8. Aiazzi B, Alparone L, Baronti S, Garzelli A (2002) Context-driven fusion of high spatial and spectral resolution images based on oversampled multi-resolution analysis. IEEE Trans Geosci Remote Sens 40(10):2300–2312

9. Chavez PS, Slides SC, Anderson JA (1991) Comparison of three different methods to merge multiresolution and multispectral data: landsat TM and SPOT panchromatic. Photogramm Eng Remote Sens 57(3):295–303
10. Pellemans A, Jordans R, Allewijn R (1993) Merging multispectral and panchromatic SPOT images with respect to the radiometric properties of the sensor. Photogramm Eng Remote Sens 59(1):81–87
11. Tu T-M, Su S-C, Shyun H-C, Huang P-S (2001) A new look at IHS-like image fusion methods. Inf Fus 2:177–186
12. Liu JG (2000) Smoothing filter-based intensity modulation: a spectral preserve image fusion technique for improving spatial details. Int J Remote Sens 21(18):3461–3472
13. Zhou J, Civco DL, Silander JA (1998) A wavelet transform method to merge landsat TM and SPOT panchromatic data. Int J Image Process 19(4):743–757
14. Wang ZJ, Ziou D, Armenakis C, Li D, Li QQ (2005) A comparative analysis of image fusion methods. IEEE Trans Geosci Remote Sens 43(6):1391–1402
15. Pajares G, de la Cruz JM (2004) A wavelet-based image fusion tutorial. Pattern Recognit 37(9):1855–1872
16. Amolins K, Zhang Y, Dare P (2007) Wavelet based image fusion techniques-an introduction, review and comparison. ISPRS J Photogramm Remote Sens 62(4):249–263
17. Lee DD, Seung HS (1999) Learning the parts of objects by non-negative matrix factorization. Nature 401:788–791
18. Jia S, Qian Y (2009) Constrained nonnegative matrix factorization for hyperspectral unmixing. IEEE Trans Geosci Remote Sens 47(1):161–173
19. Lin CJ (2007) Projected gradient methods for non-negative matrix factorization. Neural Comput 19(10):2756–2779
20. Lee DD, Seung HS (2001) Algorithms for non-negative matrix factorization. Adv Neural Inf Process Syst 13:556–562
21. Hoyer PO (2002) Non-negative sparse coding. In: Proceedings of IEEE workshop neural network. Signal process. Martigny, Switzerland, pp 557–565
22. Helmi Zulhaidi, Mohd Shafri, Affendi Suhaili, Shattri Manso (2007) The performance of maximum likelihood, spectral angle mapper. neural network and decision tree classifiers in hyperspectral image analysis. J Comput Sci 3(6):419–423
23. Nascimento JMP, Dias JMB (2005) Vertex component analysis: a fast algorithm to unmix hyperspectral data. IEEE Trans Geosci Remote Sens 43(4):898–910
24. Roberts W, Aardt JV, Ahmed F (2008) Assessment of image fusion procedures using entropy, image quality, and multispectral. J Appl Remote Sens 2:023522
25. Otazu X, Gonzalez-Audicana M, Fors O, Nunez J (2005) Introduction of sensor spectral response into image fusion methods. Application to wavelet-based methods. IEEE Trans Geosci Remote Sens 43(10):2376–2385
26. El-Mezouar MC, Taleb N, Kpalma K, Ronsin J (2011) An IHS-based fusion for color distortion reduction and vegetation enhancement in IKONOS imagery. IEEE Trans Geosci Remote Sens 49(5):1590–1602
27. Chang CI (2000) An information theoretic-based approach to spectral variability, similarity and discriminability for hyperspectral image analysis. IEEE Trans Inf Theory 46(5):1927–1932
28. Deshmukh M, Bhosale U (2010) Image fusion and image quality assessment of fused images. Int J Image Process 4(5):484–508
29. US Army Corps Engineers, http://www.tec.army.mil/hypercube/
30. China Centre for Resources Satellite Data and Application. http://www.cresda.com
31. Google Map. http://ditu.google.cn/maps